TRENDS IN SCIENCES 2026; 23(6): 12444
https://doi.org/10.48048/tis.2026.12444 RESEARCH ARTICLE

Enhanced Structural Stability of Fe_3O_4/GO–PEG Nanocomposite for Ultrasonic Pretreatment Applications

Hanif Ardhiansyah[1,2,*], Tutuk Djoko Kusworo[1] and Andri Cahyo Kumoro[1]

[1]Department of Chemical Engineering, Faculty of Engineering, Diponegoro University, Semarang 50239, Indonesia
[2]Department of Chemical Engineering, Faculty of Engineering, Universitas Negeri Semarang, Semarang 50299, Indonesia

([*]Corresponding author's e-mail: hanif.ardhi@mail.unnes.ac.id)

Received: 27 October 2025, Revised: 13 November 2025, Accepted: 20 November 2025, Published: 10 February 2026

Abstract

The development of magnetically recoverable nanocomposites with high structural stability and surface functionality is crucial for catalytic and biocatalytic processes in aqueous environments. In this work, a Fe_3O_4/GO–PEG nanocomposite was synthesized via a co-precipitation route followed by PEG functionalization to improve dispersibility, chemical robustness, and reusability. Comprehensive characterization using XRD, FTIR, TEM, BET, VSM, DLS, TGA, and ICP–OES confirmed the formation of monodisperse Fe_3O_4 nanoparticles (7 - 15 nm) uniformly anchored on GO sheets. XRD and FTIR analyses verified the Fe–O–C coordination and amide (–CO–NH–) linkages, indicating successful PEG grafting. The nanocomposite exhibited a mesoporous structure (6 - 9 nm) with a high surface area (137.4 $m^2 \cdot g^{-1}$) and retained superparamagnetic behavior (M_s = 55.8 $emu \cdot g^{-1}$), enabling rapid magnetic separation. DLS and zeta potential measurements demonstrated that PEG-induced steric stabilization effectively suppressed aggregation and reduced Fe leaching by 53% under ultrasonic conditions. The synergistic effect of GO support and PEG coating provides enhanced colloidal stability, chemical durability, and magnetic recyclability, making the material a promising platform for ultrasonic-assisted delignification and enzyme immobilization. This study establishes a clear structure–stability–function correlation in Fe_3O_4/GO–PEG systems, elucidating the critical role of PEGylation in preserving magnetism while mitigating degradation during sonochemical and biocatalytic operations.

Keywords: Fe_3O_4/GO–PEG nanocomposite, Coordination bonding, PEG functionalization, Magnetic stability, Delignification catalyst, Enzyme immobilization

Introduction

The design of stable and recyclable nanostructured catalysts has become a central goal in environmental and biochemical process engineering [1]. Magnetite (Fe_3O_4) nanoparticles possess high surface area, strong magnetic responsiveness, and redox activity, making them widely used as catalysts, supports, and separation agents in aqueous and ultrasonic-assisted reactions [2]. However, their intrinsic susceptibility to surface oxidation, aggregation and iron leaching often reduces catalytic efficiency and limits recyclability. Therefore, structural stabilization strategies are essential to preserve both magnetic functionality and catalytic performance during repeated operation [3].

Graphene oxide (GO) provides an excellent platform for dispersing and anchoring Fe_3O_4 nanoparticles due to its two-dimensional structure, high surface area, and abundant oxygenated functional groups (–COOH, –OH and epoxide) [4]. These sites enable the formation of Fe–O–C coordination bonds, ensuring homogeneous particle distribution and improved interfacial adhesion [5]. Nevertheless, Fe_3O_4/GO composites often suffer from colloidal instability and partial Fe leaching in liquid environments, indicating the need for surface passivation [6].

To address these drawbacks, surface modification using hydrophilic polymers—particularly polyethylene glycol (PEG)—has proven effective in improving dispersion and long-term stability of nanocomposites [7,8]. PEG, a nonionic polymer with terminal hydroxyl or amine groups, forms hydration layers and covalent or coordinative bonds with oxygenated sites on Fe_3O_4 or GO surfaces [9]. This steric protection prevents magnetic dipole-induced aggregation and simultaneously enhances compatibility in aqueous or biocatalytic systems [10,11].

Recent studies have shown that Fe_3O_4/GO–PEG composites exhibit remarkable reusability, reduced iron leaching, and superior stability under both sonochemical and oxidative conditions. PEGylation forms a thin protective layer (3 - 5 nm) that effectively suppresses Fe^{2+}/Fe^{3+} oxidation–dissolution cycles while preserving the superparamagnetic nature of Fe_3O_4 [12]. Despite these advances, the underlying structure–property relationships governing the physicochemical stability and magnetic behavior of Fe_3O_4/GO–PEG nanocomposites remain insufficiently explored. A deeper understanding of the interactions among crystallinity, interfacial bonding, and surface chemistry is essential to optimize their performance in catalytic and enzyme immobilization systems [13]. Fe_3O_4/GO-based composites, in general, are widely applied in catalytic and magnetically assisted processes because of their high surface area and tunable surface chemistry [14,15]. The presence of strong interfacial bonding and functionalized surfaces enhances their operational stability under both oxidative and ultrasonic environments. Moreover, PEG-modified magnetic composites have been consistently reported to display improved dispersion and chemical durability [16,17]. These hybrid systems integrate the magnetic responsiveness of Fe_3O_4 with the steric shielding effect of PEG, effectively minimizing aggregation and extending catalytic lifetime in aqueous or reactive media [18].

In this study, Fe_3O_4/GO–PEG nanocomposites were synthesized via a co-precipitation method followed by PEG-assisted functionalization. Comprehensive characterization techniques, including XRD, FTIR, TEM, BET–BJH, VSM, DLS–zeta potential, TGA–DTG and ICP–OES, were employed to elucidate their structure, morphology and stability. This work aims to establish a clear correlation between synthesis, structural features and stability behavior, thereby revealing the mechanism by which PEG-induced surface modification enhances magnetic retention, dispersion and resistance to Fe leaching. The resulting insights are expected to support future application of Fe_3O_4/GO–PEG as a recyclable catalyst and enzyme carrier in ultrasonic-assisted delignification and bioconversion processes.

Materials and methods

Materials

Iron (III) chloride hexahydrate ($FeCl_3 \cdot 6H_2O$, ≥ 99%), iron (II) chloride tetrahydrate ($FeCl_2 \cdot 4H_2O$, ≥ 98%), sulfuric acid (H_2SO_4, ACS grade), ethanol (≥ 99.8%) and single-layer graphene oxide (GO, > 95%) were purchased from Sigma-Aldrich (St. Louis, MO, USA). Amino-functionalized polyethylene glycol (PEG–NH_2, Mw 6000), 1-ethyl-3-(3-dimethylaminopropyl) carbodiimide hydrochloride (EDC·HCl, ≥ 98%), N-hydroxysuccinimide (NHS, 98%), 2-(N-morpholino) ethanesulfonic acid (MES, ≥ 99%), and ammonium hydroxide (NH_4OH, 28%) were obtained from Merck (Darmstadt, Germany). Ultrapure water (resistivity ≥ 18.2 MΩ·cm, 25 °C) from a Millipore Milli-Q system was used in all experiments.

Methods

Synthesis of Fe_3O_4 nanoparticles

Fe_3O_4 nanoparticles were synthesized using a modified co-precipitation method under nitrogen atmosphere. $FeCl_3 \cdot 6H_2O$ (3.25 g, 12 mmol) and $FeCl_2 \cdot 4H_2O$ (1.19 g, 6 mmol) were dissolved in 100 mL deionized water, purged with nitrogen for 15 min to prevent Fe^{2+} oxidation and heated to 80 ± 1 °C under stirring (500 rpm). A 28% NH_4OH solution was added dropwise (2 mL·min^{-1}) until pH reached 10.5 ± 0.1. The suspension was maintained for 1 h under N_2 to ensure complete precipitation. The resulting black precipitate was magnetically separated, washed with ethanol and deionized water until neutral pH, and vacuum-dried at 60 °C for 12 h.

The overall reaction can be expressed as:

$$Fe^{2+} + 2Fe^{3+} + 8OH^- \rightarrow Fe_3O_4 + 4H_2O \quad (1)$$

Synthesis of Fe_3O_4/GO nanocomposite

Graphene oxide (50 mg) was dispersed in 50 mL of deionized water via ultrasonication (40 kHz, 150 W, 30 min; Branson 5800, USA) to obtain a stable colloidal suspension. The dispersion step facilitated complete exfoliation of GO sheets and uniform distribution within the aqueous phase. AFM analysis was not performed in this study; instead, the GO sheet dimensions were adopted from previously reported works synthesized under similar oxidation and exfoliation conditions [19-21].

Fe_3O_4 nanoparticles (100 mg, corresponding to a 2:1 mass ratio to GO) were then added to the GO dispersion under continuous nitrogen flow. The mixture was mechanically stirred at 70 ± 2 °C for 2 h to promote electrostatic and coordinative interactions between Fe_3O_4 and the oxygen-containing functional groups of GO. During this process, Fe_3O_4 nanoparticles were anchored onto GO sheets through Fe–O–C coordination bonds, forming a homogeneous nanocomposite suspension. The resulting Fe_3O_4/GO nanocomposite was magnetically separated, rinsed three times with ethanol (30 mL each) to remove unbound particles and impurities, and subsequently dried at 60 °C under vacuum for 12 h to obtain a fine black powder ready for subsequent PEG functionalization.

Covalent PEGylation of Fe_3O_4/GO

The Fe_3O_4/GO composite (40 mg) was dispersed in 20 mL MES buffer (50 mM, pH 6.0) containing EDC (50 mM) and NHS (25 mM) for 30 min at 25 °C to activate carboxyl groups on GO. Amino-functionalized PEG (200 mg, Fe:GO:PEG ≈ 6:1:2) was then added and stirred for 24 h at 25 °C to form amide bonds between PEG–NH_2 and activated –COOH sites. The product was magnetically separated, thoroughly washed with deionized water, and freeze-dried (–80 °C, 24 h). Successful PEGylation was confirmed by FTIR (amide I and II bands at ~1,650 and 1,550 cm^{-1}) and TGA showing ~10 wt% increased organic fraction.

Characterization techniques

X-ray diffraction (XRD)

Phase identification and structural analysis of the synthesized materials were conducted using a Bruker D8 Advance X-ray diffractometer equipped with a LynxEye detector. The instrument operated with Cu-Kα radiation (λ = 1.5406 Å) generated at 40 kV and 40 mA. Diffraction data were collected in the 2θ range of 10° - 80° at a step size of 0.02°.

The obtained peaks were indexed based on JCPDS standards to confirm the spinel Fe_3O_4 phase and investigate the structural influence of GO and PEG incorporation. Crystallite size (D) was calculated using the Scherrer Eq. (2).

$$D = \frac{K\lambda}{\beta \cos\theta} \quad (2)$$

where D represents the mean crystallite size, K is the shape factor (0.9), λ is the X-ray wavelength, β is the line broadening at half the maximum intensity (FWHM) in radians and θ is the Bragg angle.

The Williamson-Hall analysis was employed to separate the contributions of crystallite size and lattice strain to peak broadening Eq. (3).

$$\beta \cos\theta = \frac{K\lambda}{D} + 4\varepsilon \sin\theta \quad (3)$$

where ε represents the lattice strain.

Transmission electron microscopy (TEM)

The morphology and microstructure of the nanocomposites were examined using a JEOL JEM-2100 transmission electron microscope operating at 200 kV. Samples were prepared by dispersing the powder in ethanol, ultrasonicated for 10 min and drop-cast onto carbon-coated copper grids. TEM images provided direct evidence of Fe_3O_4 nanoparticle dispersion on GO sheets, the presence of PEG coating layers and the average particle size distribution, which were correlated with XRD-derived crystallite sizes. High-resolution TEM (HRTEM) micrographs and selected-area electron diffraction (SAED) patterns were used to confirm the spinel structure and crystallographic orientation of Fe_3O_4 nanoparticles.

Fourier-transform infrared spectroscopy (FTIR)

Fourier-transform infrared (FTIR) spectra were recorded using a Shimadzu IRTracer-100 spectrometer within the wavenumber range of 4,000 - 400 cm^{-1} (resolution 4 cm^{-1}). The samples were prepared as KBr pellets and analyzed to identify characteristic functional

groups and confirm chemical bonding interactions between Fe_3O_4, GO and PEG. The presence of Fe–O, C=O and C–O–C stretching vibrations was used to verify the successful grafting of PEG onto the Fe_3O_4/GO surface.

Vibrating sample magnetometry (VSM)

Magnetic properties were investigated using a Lake Shore 7407 vibrating sample magnetometer at room temperature with an applied magnetic field up to ± 10 kOe. The magnetization (M) versus field (H) curves were analyzed to determine the saturation magnetization (Ms), coercivity (Hc), and remanence (Mr). The data were used to evaluate the superparamagnetic behavior and the effect of GO and PEG modification on magnetic response, which is essential for catalyst recyclability.

Dynamic light scattering (DLS) and zeta potential

The hydrodynamic diameter and zeta potential of Fe_3O_4/GO and Fe_3O_4/GO–PEG nanocomposites were measured using a Zetasizer Nano ZS (Malvern Instruments, UK) at 25 °C. Each sample (0.1 mg mL^{-1}) was dispersed in deionized water and ultrasonicated (100 W, 10 min) prior to measurement. The results were obtained as the average of three replicates. The DLS analysis provided the mean particle size distribution, while the zeta potential indicated the surface charge and colloidal stability in aqueous suspension.

Brunauer–emmett–teller (BET) and Barrett–joyner–halenda (BJH) analyses

The specific surface area, pore volume, and pore size distribution were determined using N_2 adsorption–desorption isotherms measured at 77 K on a Quantachrome NOVA 2200e surface area analyzer. Samples were degassed under vacuum at 150 °C for 6 h before measurement. The BET model was used to determine the surface area, while the BJH method was applied to evaluate the pore structure and confirm the mesoporosity characteristics. These results were used to correlate textural parameters with catalytic and enzyme immobilization potential.

Thermogravimetric and derivative thermogravimetric analysis (TGA–DTG)

Thermal stability and compositional analysis were performed using a Mettler Toledo TGA/DSC 1 analyzer under N_2 atmosphere. Approximately 10 mg of sample was heated from 30 to 800 °C at a rate of 10 °C·min^{-1}.

The TGA and DTG curves were used to determine the decomposition stages, total organic content, and thermal stability of the composites. Weight loss steps were correlated with moisture removal, oxidation of GO functional groups, and PEG degradation, confirming successful polymer incorporation and enhanced thermal endurance.

Iron leaching test (ICP–OES)

The iron leaching stability of Fe_3O_4/GO and Fe_3O_4/GO–PEG nanocomposites was evaluated using Inductively Coupled Plasma–Optical Emission Spectroscopy (ICP–OES, Agilent 5110, USA). Approximately 50 mg of catalyst was dispersed in 100 mL of deionized water and subjected to ultrasonication (250 W, 30 min, 50 °C). The sonication parameters (250 W, 30 min, 50 °C) were determined through internal optimization experiments to achieve homogeneous dispersion and stable cavitation without overheating or causing structural degradation. Lower power (<200 W) resulted in incomplete particle dispersion, whereas higher power (>300 W) induced partial aggregation and increased Fe dissolution. Therefore, the selected parameters provided optimal energy input for assessing Fe leaching behavior under representative ultrasonic pretreatment conditions.

After sonication, the suspension was magnetically separated, and the supernatant was analyzed for Fe concentration using ICP–OES at a wavelength of 238.204 nm. The Fe concentration (ppm) was used to quantify the leaching percentage and evaluate the structural integrity and chemical resistance of the nanocomposites under ultrasonic exposure.

Quality control and reproducibility

All experimental procedures were conducted in triplicate to ensure reproducibility, and the measurement uncertainty for all analytical data was maintained within ± 5%. The obtained results represent the mean values of three independent trials with standard deviations below

5%, confirming the reliability and consistency of the experimental methodology.

Results and discussion

Structural and morphological characterization of Fe_3O_4/GO-PEG nanocomposite

X-ray diffraction analysis

The crystalline structure of the synthesized Fe_3O_4/GO–PEG nanocomposite was examined by X-ray diffraction (XRD); the diffractogram is shown in **Figure 1**. Diffraction peaks at 2θ = 30.1°, 35.6°, 43.3°, 53.6°, 57.1° and 62.6° correspond to the (220), (311), (400), (422), (511) and (440) planes of magnetite (Fe_3O_4), consistent with the cubic inverse spinel (ICDD PDF No. 19-0629). A peak at 26.5° assigned to the (002) plane confirms the presence of graphene oxide (ICDD PDF No. 41-1487). No peaks attributable to maghemite (γ-Fe_2O_3) or hematite (α-Fe_2O_3) were observed, indicating high phase purity and the effectiveness of nitrogen protection during synthesis [22-24].

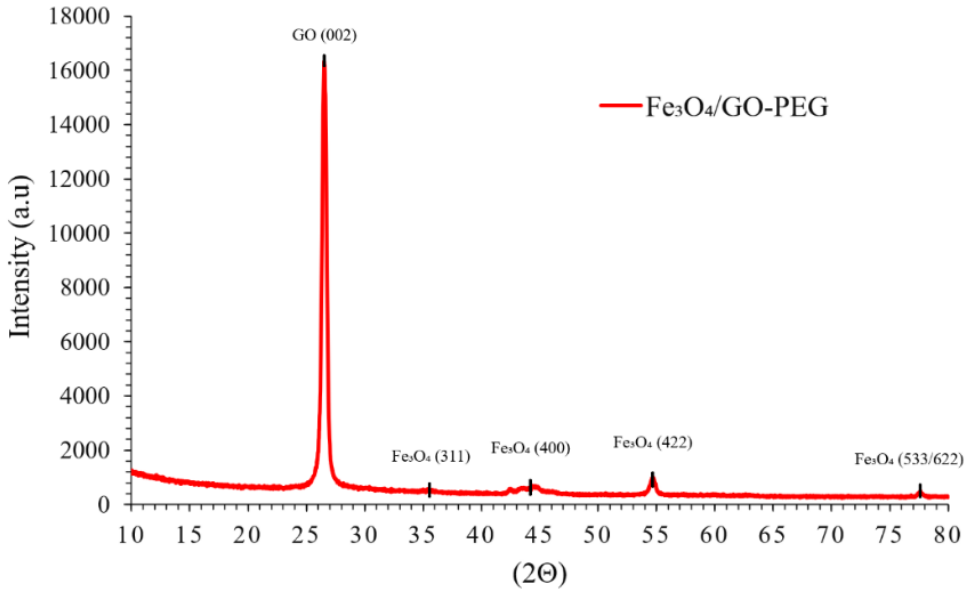

Figure 1 XRD patterns of the Fe_3O_4/GO-PEG nanocomposite.

A small positive shift in Fe_3O_4 peak positions (average $\Delta 2\theta \approx +0.15°$) and a reduced d-spacing indicate mild lattice contraction, likely induced by interfacial strain and charge transfer between Fe_3O_4 and GO oxygenated sites. The refined lattice parameter (a = 8.376 Å) is slightly smaller than standard Fe_3O_4 (a = 8.396 Å), corresponding to ~ 0.24% contraction and consistent with Fe–O–C interfacial interactions [25]. Peak broadening was quantified using the Scherrer equation and Williamson–Hall analysis after instrumental correction with a Si standard (NIST SRM 640c) [26]. The average crystallite size is 7.6 ± 0.3 nm and the microstrain $\varepsilon \approx 3.2\times10^{-3}$. The presence of GO and PEG likely constrained crystal growth through spatial confinement and steric stabilization during nucleation [27].

Rietveld refinement confirms the dominance of the Fe_3O_4 phase (94.3 wt%) with minor surface oxidation to γ-Fe_2O_3 (2.8 wt%) and ~2.9 wt% amorphous carbonaceous content ascribed to GO–PEG. Refinement quality factors (Rwp = 8.2%, χ^2 = 1.26) indicate a good fit between the experimental and simulated patterns. The observed low oxidation level—substantially lower than values reported for uncoated Fe_3O_4 (8 - 15 wt%)—supports the protective role of the GO–PEG coating in preserving phase stability. The refined structural and microstructural parameters are summarized in **Table 1** and quantitatively confirm uniform nanoscale crystallinity, slight lattice contraction, and high phase purity for the Fe_3O_4/GO–PEG nanocomposite [28].

Table 1 Structural parameters derived from Rietveld refinement of Fe_3O_4/GO–PEG nanocomposite.

Parameter	Observed Value	Standard Fe_3O_4	Δ (%)	Interpretation
Lattice parameter, a (Å)	8.376 ± 0.003	8.396	–0.24	Lattice contraction
Crystallite size (nm)	7.6 ± 0.3	-	-	Nanoscale Fe_3O_4 domains
Microstrain ($\varepsilon \times 10^{-3}$)	3.2	-	-	Interfacial lattice distortion
Phase composition (wt%)	Fe_3O_4: 94.3 / γ-Fe_2O_3: 2.8 / Amorphous: 2.9	-	-	High phase purity

Transmission electron microscopy analysis

Transmission electron microscopy (TEM) provided direct morphological evidence of nanoparticle distribution and interfacial interactions among Fe_3O_4, GO and PEG components. As shown in **Figure 2**, spherical Fe_3O_4 nanoparticles with diameters ranging from 7 - 15 nm are uniformly anchored on GO sheets. This size range corresponds well with the crystallite size obtained from Scherrer and Williamson–Hall analyses (~7.6 nm), confirming that the nanoparticles are primarily monocrystalline [29]. Minor local clustering is observed, which can be attributed to weak magnetic dipole–dipole and van der Waals attractions rather than actual sintering, since the primary particle boundaries remain intact. Such limited aggregation is typical for magnetic nanomaterials and does not compromise nanoscale uniformity [30].

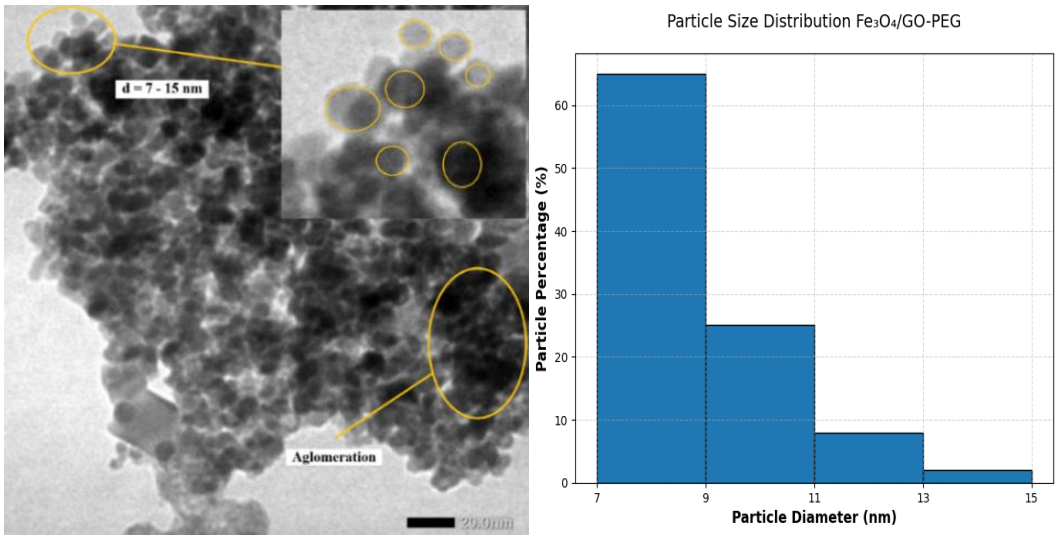

Figure 2 TEM image of Fe_3O_4/GO–PEG nanocomposite showing uniformly distributed spherical Fe_3O_4 nanoparticles (7 - 15 nm) anchored on graphene oxide sheets.

The homogeneous dispersion of Fe_3O_4 nanoparticles is facilitated by oxygenated functional groups on GO (–COOH, –OH and C–O–C), which act as active nucleation and anchoring sites for Fe^{2+}/Fe^{3+} ions during co-precipitation. These groups promote coordination and electrostatic interactions, leading to the formation of Fe–O–C linkages that inhibit uncontrolled growth and aggregation. The wrinkled morphology of GO, evident in **Figure 3**, results from oxidation-induced defects that introduce local curvature and strain, providing additional anchoring sites for nanoparticle attachment. This structural feature enhances surface area and promotes strong interfacial adhesion between Fe_3O_4 and GO [31,32].

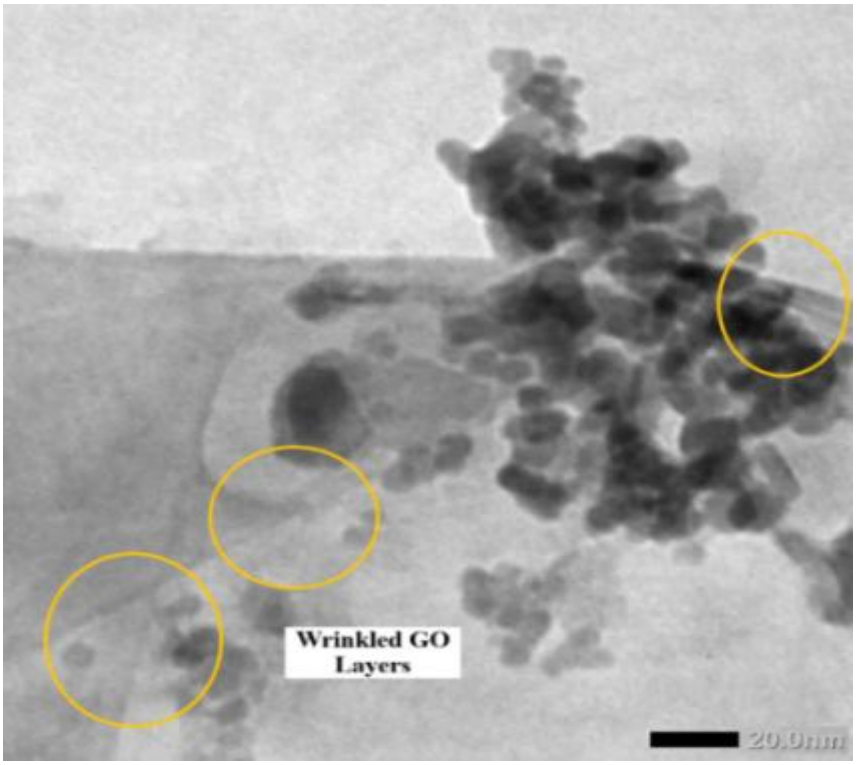

Figure 3 TEM image of wrinkled graphene oxide morphology with surface-anchored Fe_3O_4 nanoparticles, highlighting sheet flexibility and nanoparticle adhesion.

The interfacial attachment between Fe_3O_4 and GO likely involves multiple bonding mechanisms. Coordination bonding occurs between Fe^{3+} ions and oxygenated groups ($–COO^-$, –O–) on GO, producing stable Fe–O–C linkages. In addition, π–d orbital hybridization between Fe_3O_4 and the π-system of GO may enhance charge transfer across the interface. For the PEG-functionalized system, crosslinking occurs through amide bond formation between GO–COOH and NH_2-terminated PEG chains, providing additional interfacial flexibility and stability [33].

The effect of PEG modification is clearly observed when comparing **Figures 4(a) - 4(b)**. In **Figure 4(a)**, a faint amorphous halo (~3 - 5 nm thick) surrounding Fe_3O_4 nanoparticles indicates the presence of a PEG coating. This diffuse contrast, originating from the polymer's low electron density, provides direct visual evidence of PEG encapsulation. The PEG shell forms a hydrated steric barrier that reduces magnetic dipole interactions and prevents nanoparticle agglomeration, thereby improving colloidal stability in aqueous media. Conversely, the unmodified Fe_3O_4/GO sample (**Figure 4(b)**) lacks this halo and exhibits denser nanoparticle clustering, confirming that PEG is essential for suppressing magnetic aggregation.

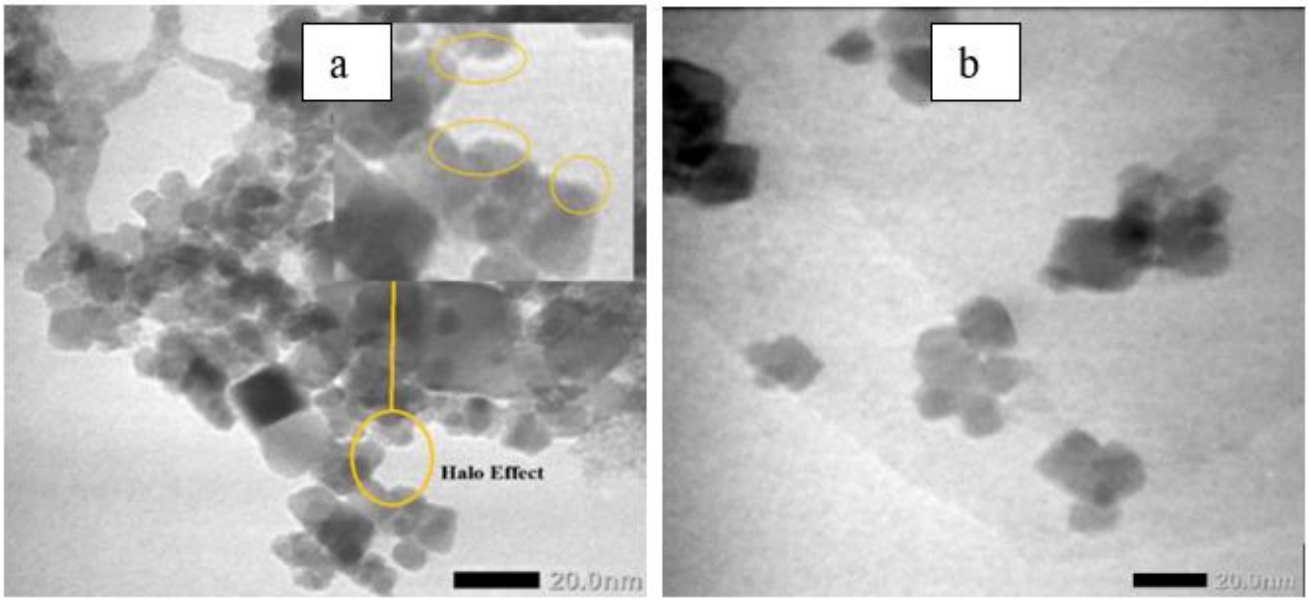

Figure 4 (a) TEM image showing amorphous PEG "halo" surrounding Fe_3O_4 nanoparticles on GO (indicating polymer coating). (b) TEM image of Fe_3O_4/GO without PEG coating, showing denser aggregation and absence of halo contrast.

This morphological comparison highlights the dual role of PEG as both a steric stabilizer and surface modifier. PEG chains establish hydrophilic interfaces and impart long-range repulsive forces, maintaining uniform dispersion without altering the crystalline nature of Fe_3O_4 or the layered morphology of GO. These TEM observations, consistent with XRD and BET results, confirm that PEG functionalization preserves nanoscale integrity, uniform particle distribution, and robust interfacial compatibility—key attributes for catalytic and enzyme-immobilization applications [34].

Although scanning electron microscopy (SEM) was not conducted, the surface morphology inferred from TEM and BET–BJH analyses indicates that Fe_3O_4 nanoparticles are uniformly distributed over the wrinkled GO surface with minimal aggregation. This nanoscale architecture corresponds well with the mesoporous texture and homogeneous surface area derived from BET analysis. Similar morphologies have been reported for Fe_3O_4/GO–PEG nanostructures stabilized by polymeric modifiers [35,36], reinforcing that PEG functionalization enhances interfacial adhesion, smooth surface coverage, and stable dispersion in aqueous systems.

Fourier transform infrared spectroscopy analysis

Fourier-transform infrared (FTIR) spectroscopy was employed to verify interfacial interactions among Fe_3O_4, graphene oxide (GO), and polyethylene glycol (PEG), and to confirm successful surface functionalization of the Fe_3O_4/GO–PEG nanocomposite [37,38]. The FTIR spectra of Fe_3O_4, Fe_3O_4/GO and Fe_3O_4/GO–PEG are presented in **Figure 5**, while the key vibrational assignments and spectral shifts are summarized in **Tables 2** and **3**.

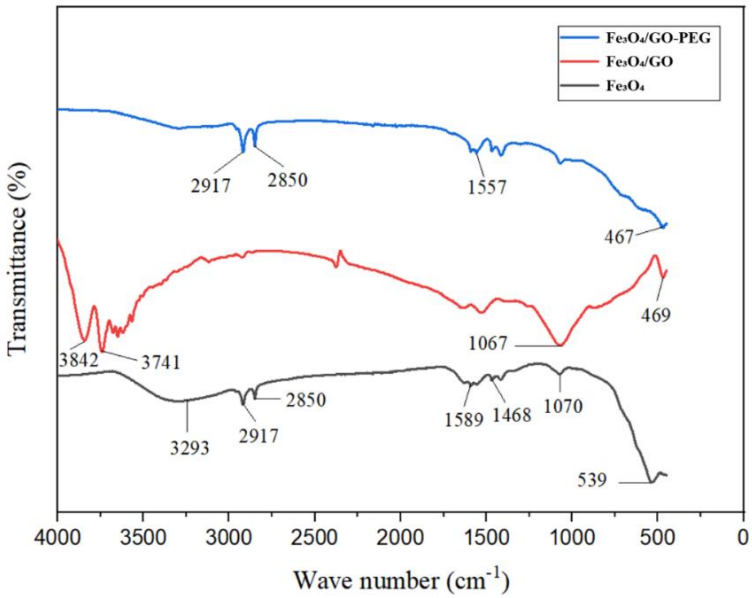

Figure 5 FTIR Spectra of Fe_3O_4, Fe_3O_4/GO, and Fe_3O_4/GO-PEG Nanocomposites.

The spectrum of pristine Fe_3O_4 exhibits a characteristic Fe–O stretching vibration near 540 cm^{-1}, typical of the spinel lattice structure. Two broad absorption bands at 3,290 cm^{-1} (O–H stretching) and 1,635 cm^{-1} (H–O–H bending) correspond to surface hydroxyls and adsorbed water molecules, confirming the hydrated surface of magnetite [39]. Upon hybridization with GO, new absorption bands emerge, and notable frequency shifts occur. The Fe–O vibration redshifts from 540 to ~470 cm^{-1}, indicating the formation of interfacial Fe–O–C coordination bonds between Fe_3O_4 and GO oxygenated groups. Additional peaks at 1,625 cm^{-1} (C=C stretching) and 1,060 cm^{-1} (C–O–C stretching) confirm the incorporation of GO's functional moieties into the composite. The substantial Fe–O shift ($\Delta\nu \approx -70$ cm^{-1}), which exceeds the typical physisorption range (5 - 15 cm^{-1}), evidences strong chemical coupling at the Fe_3O_4/GO interface—consistent with the lattice contraction observed in XRD analysis [6].

Table 2 Comparative FTIR peak positions of Fe_3O_4, Fe_3O_4/GO, and Fe_3O_4/GO–PEG nanocomposites.

Functional group/Vibration	**Fe_3O_4 (cm^{-1})**	**Fe_3O_4/GO (cm^{-1})**	**Fe_3O_4/GO–PEG (cm^{-1})**	**Assignment/ Structuralchange**
Fe–O stretching	540	470	467	Redshift → Fe–O–C coordination bond formation
O–H stretching	3,290	3,316	3,343	Blueshift → Strengthened H-bonding network
H–O–H bending	1,635	1,625	-	Reduced intensity → dehydration after GO incorporation
C=C stretching	-	1,625	1,651	Slight shift → Amide I / conjugation with C=O
C–O–C stretching	-	1,060	1,055	Stable → Retained GO epoxy/alkoxy groups
CH_2 stretching	-	-	2,918, 2,851	New → PEG incorporation
N–H bending	-	-	1,557	New → Amide II (PEG–NH_2 coupling)

After PEG modification, two new absorption bands at 2,918 and 2,851 cm^{-1} (CH_2 asymmetric/symmetric stretching) confirm the introduction of PEG chains. The amide I (1,651 cm^{-1}) and amide II (1,557 cm^{-1}) bands verify covalent linkage between GO carboxyl groups and PEG–NH_2, mediated by EDC/NHS coupling chemistry. A slight Fe–O shift from 470 to ~467 cm^{-1} suggests additional coordination between surface Fe atoms and PEG oxygen atoms, indicating PEG's role as a mild surface passivator enhancing chemical and structural stability [40].

Table 3 Key vibrational shifts and chemical interpretations.

Structural transition	Observed shift (cm^{-1})	Interpretation
Fe–O: 540 → 470 → 467	Large redshift (–73)	Formation of Fe–O–C bonds between Fe_3O_4 and GO/PEG
O–H: 3290 → 3343	Blueshift (+53)	Formation of extended H-bonding with PEG hydroxyls
C=O (GO): 1,730 → disappears	Band loss	Carboxyl groups are consumed in amide bond formation
CH_2 and Amide (PEG): New 2918, 2851, 1651, 1557	-	Covalent PEG attachment confirmed
C–O–C (GO): Stable 1060 → 1055	Slight shift	GO structure retained; partial interaction with PEG

These progressive spectral transformations reveal a stepwise structural evolution from Fe_3O_4 → Fe_3O_4/GO → Fe_3O_4/GO–PEG, driven by both coordination and covalent bonding mechanisms. The Fe–O redshift confirms Fe–O–C linkage formation, while the emergence of amide and CH_2 vibrations verifies successful PEGylation. Additionally, the O–H blueshift (+47 cm^{-1}) suggests a reinforced hydrogen-bonding network involving Fe_3O_4 surface hydroxyls, GO oxygen functionalities and PEG hydroxyl groups [9].

This multilevel bonding framework enhances structural integrity, hydrophilicity, and dispersion stability, correlating directly with the improved colloidal behavior and reduced Fe leaching observed in DLS and ICP–OES analyses. Collectively, these results demonstrate that the Fe_3O_4/GO–PEG nanocomposite integrates Fe–O–C coordination, covalent amide linkages, and hydrogen-bond interactions, resulting in superior interfacial cohesion and magnetic recyclability—key attributes for catalytic and enzyme immobilization applications [41].

BET surface area and porosity

The N_2 adsorption–desorption isotherms of Fe_3O_4/GO and Fe_3O_4/GO–PEG nanocomposites are shown in **Figure 6(a)**. Both materials exhibit Type IV isotherms with H_3 hysteresis loops, according to IUPAC classification, indicating the presence of mesoporous structures formed by slit-shaped pores originating from stacked graphene oxide layers and interparticle voids among Fe_3O_4 nanoparticles [42].

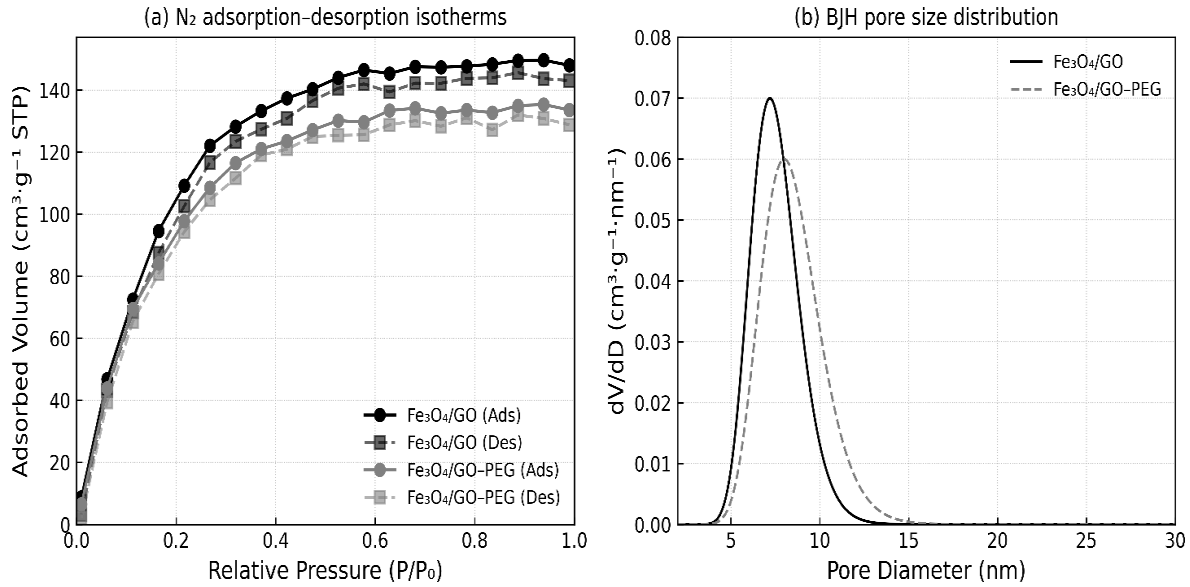

Figure 6 (a) N_2 adsorption–desorption isotherms and (b) BJH pore size distribution curves of Fe_3O_4/GO and Fe_3O_4/GO–PEG nanocomposites.

For the Fe_3O_4/GO sample, the adsorption branch shows a steep increase at relative pressure (P/P_0) >0.4, followed by a broad hysteresis loop, confirming the mesoporous nature of the composite associated with capillary condensation. After PEG modification, the Fe_3O_4/GO–PEG nanocomposite displays a similar isotherm profile but with slightly reduced adsorbed volume. This decrease suggests that PEG molecules partially occupy or block pore channels while maintaining the overall mesoporous structure [43].

As summarized in **Table 4**, the BET surface area of Fe_3O_4/GO is 152.8 $m^2 \cdot g^{-1}$, which decreases slightly to 137.4 $m^2 \cdot g^{-1}$ after PEG functionalization. Similarly, the total pore volume (V_p) drops from 0.276 to 0.247 $cm^3 \cdot g^{-1}$, while the average pore diameter (D_p) shifts marginally from 7.15 to 6.82 nm. These reductions can be attributed to partial surface coverage by PEG chains, which introduce steric hindrance and limit N_2 adsorption without collapsing the mesoporous framework [44].

Table 4 BET and BJH parameters of Fe_3O_4/GO and Fe_3O_4/GO–PEG nanocomposites.

Sample	BET Surface area ($m^2 \cdot g^{-1}$)	Total pore volume ($cm^3 \cdot g^{-1}$)	Average pore diameter (nm)	Pore type (BJH)
Fe_3O_4/GO	152.8	0.276	7.15	Mesoporous (H_3)
Fe_3O_4/GO–PEG	137.4	0.247	6.82	Mesoporous (H_3)

The BJH pore size distribution curves (**Figure 6(b)**) show a narrow mesopore range of 6 - 9 nm, confirming that both composites retain a uniform mesoporous texture suitable for catalytic and enzyme immobilization applications. The slight shift toward smaller average pore diameters after PEG incorporation is consistent with partial pore coverage and possible expansion of the GO interlayer spacing due to flexible PEG chains [45]. Overall, PEG modification provides a balance between structural stability, mesoporosity, and surface accessibility—three key parameters determining catalytic and functional performance. Although PEG slightly decreases surface area and pore volume, it effectively preserves mesoporosity and enhances stability, making Fe_3O_4/GO–PEG nanocomposites well-suited for catalytic and enzyme immobilization processes [46].

Magnetic properties (VSM)

The magnetic hysteresis loops of Fe_3O_4, Fe_3O_4/GO, and Fe_3O_4/GO–PEG nanocomposites are shown in **Figure 7**. All samples exhibit typical superparamagnetic behavior, characterized by S-shaped magnetization curves with negligible coercivity (Hc < 50 Oe) and remanence (Mr ≈ 0). This superparamagnetic nature allows easy magnetization and demagnetization, a crucial property for recyclable nanocatalysts [47].

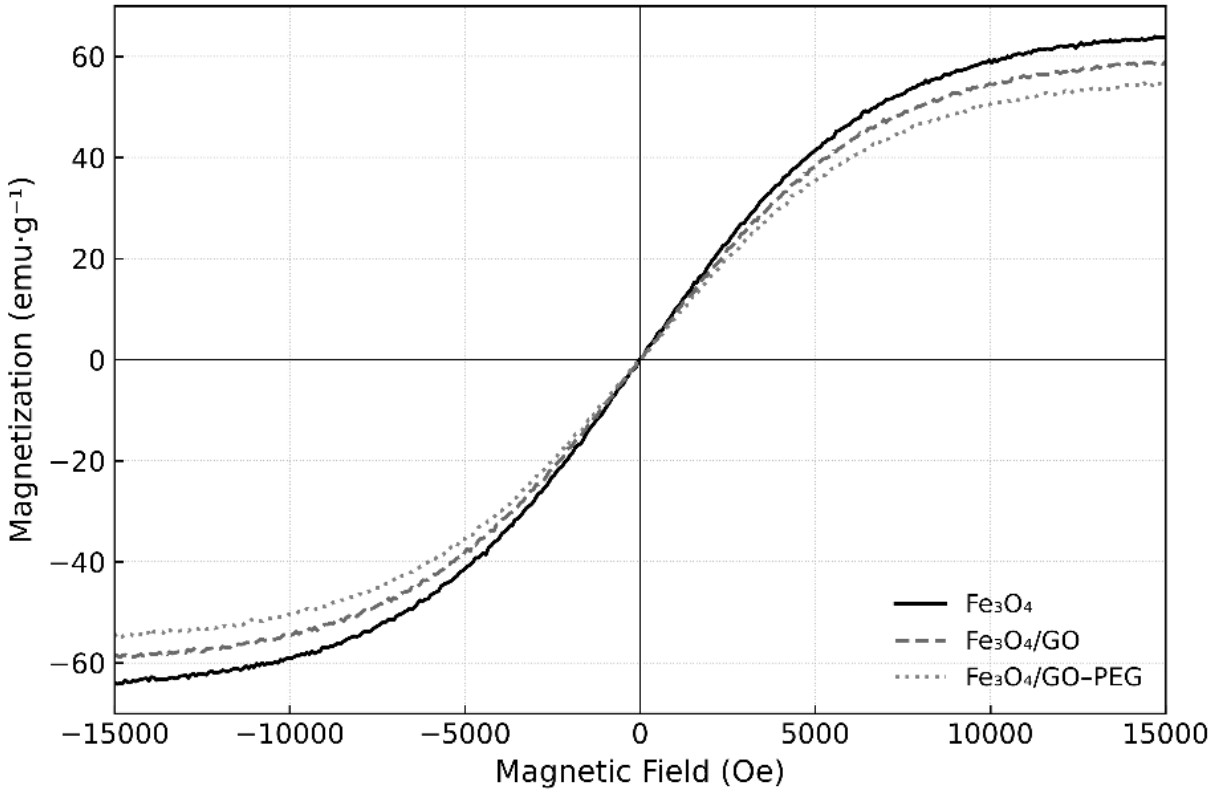

Figure 7 Magnetic hysteresis loops of Fe_3O_4, Fe_3O_4/GO, and Fe_3O_4/GO–PEG nanocomposites measured at 298 K.

The saturation magnetization (M_s) values summarized in **Table 5** reveal a systematic decrease upon surface modification. Pure Fe_3O_4 displays the highest M_s of 65.3 emu·g^{-1}, which decreases to 60.2 emu·g^{-1} after GO incorporation and further to 55.8 emu·g^{-1} following PEG functionalization. This reduction arises from the introduction of nonmagnetic GO and PEG components, which increase the total mass of the composite without contributing to its magnetic moment. Despite this decrease, the Fe_3O_4/GO–PEG nanocomposite retains sufficient magnetic strength for rapid magnetic separation (<10 s) using a standard Nd–Fe–B magnet [48].

Table 5 Magnetic parameters derived from VSM measurements.

Sample	M_s (emu·g^{-1})	Mr (emu·g^{-1})	Hc (Oe)	Magnetic behavior
Fe_3O_4	65.3	0.78	46.1	Superparamagnetic
Fe_3O_4/GO	60.2	0.65	42.5	Superparamagnetic
Fe_3O_4/GO–PEG	55.8	0.61	40.8	Superparamagnetic

The preserved magnetic hysteresis shape and low coercivity indicate that PEG functionalization does not disrupt the Fe_3O_4 spinel lattice or its superparamagnetic character, consistent with XRD and FTIR analyses. Furthermore, the PEG coating improves colloidal stability and reusability of the nanocomposite in aqueous and ultrasonic environments by mitigating magnetic aggregation and oxidation [49]. Overall, these results confirm that PEG modification introduces a nonmagnetic but stabilizing interface that balances magnetic responsiveness with improved durability and dispersion—key properties for magnetically recoverable nanocatalysts.

Dynamic Light Scattering (DLS) and zeta potential analysis

The hydrodynamic diameter and surface charge of Fe_3O_4/GO and Fe_3O_4/GO–PEG nanocomposites were analyzed to evaluate their colloidal behavior in aqueous suspension (**Figures 8(a) - 8(b)**). As shown in **Figure 8(a)**, the particle size distribution shifts toward a larger average hydrodynamic diameter after PEG modification—from 185 ± 8 nm for Fe_3O_4/GO to 220 ± 10 nm for Fe_3O_4/GO–PEG. This increase reflects the formation of a hydrated PEG shell surrounding the nanocomposite surface, which enlarges the apparent particle diameter due to solvation and steric expansion [50]. In addition, the polydispersity index (PDI) decreases from 0.21 to 0.18, indicating narrower size distribution and improved dispersion uniformity.

Meanwhile, **Figure 8(b)** presents the corresponding zeta potential (ζ) values, showing a shift from –22.4 mV for Fe_3O_4/GO to –8.3 mV for Fe_3O_4/GO–PEG. The reduced magnitude of surface charge arises from partial masking of oxygenated groups (–COOH, –OH) on GO by the PEG chains. Although the absolute ζ value decreases, overall colloidal stability improves significantly, attributed to the steric hindrance provided by PEG's flexible ether and hydroxyl groups [51].

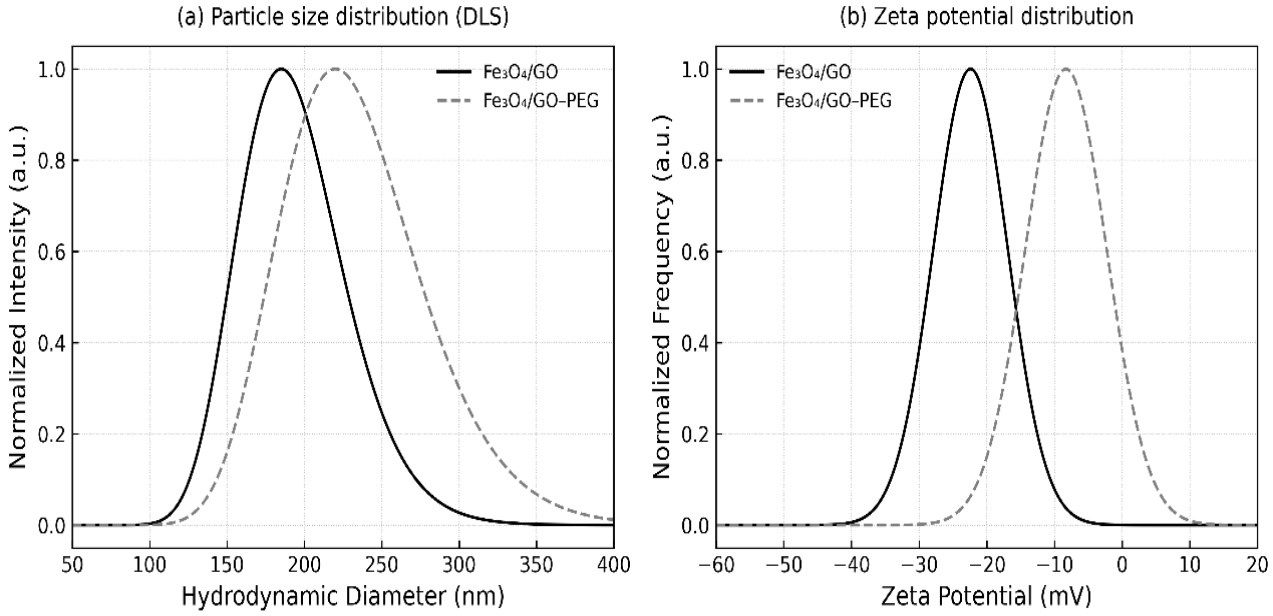

Figure 8 (a) Particle size distribution and (b) zeta potential of Fe_3O_4/GO and Fe_3O_4/GO–PEG nanocomposites.

According to the extended DLVO theory, the steric repulsion introduced by PEG chains counteracts the attractive van der Waals forces, resulting in a net positive interaction potential that prevents particle aggregation. Visually, the Fe_3O_4/GO–PEG dispersion remained stable for more than seven days, whereas Fe_3O_4/GO showed noticeable sedimentation within 24 h [52]. These findings confirm that PEG functionalization introduces a dominant steric stabilization mechanism that overrides electrostatic effects, ensuring long-term colloidal stability, which is essential for liquid-phase catalytic and enzymatic applications. PEG modification simultaneously increases the hydrodynamic diameter and decreases the magnitude of the surface charge,

thereby transitioning from electrostatic to steric stabilization and improving dispersion durability in aqueous media [53].

Thermal stability (TGA-DTG Analysis)

Thermogravimetric (TGA) and derivative thermogravimetric (DTG) analyses were performed to assess the thermal stability, organic content, and decomposition profile of Fe_3O_4/GO and Fe_3O_4/GO–PEG nanocomposites. The combined TGA–DTG curves, presented in **Figure 9**, reveal distinct multi-step weight loss behavior typical of organic–inorganic hybrid systems. As observed in the figure, the Fe_3O_4/GO–PEG sample exhibits three decomposition stages, whereas Fe_3O_4/GO undergoes two primary weight-loss events [54].

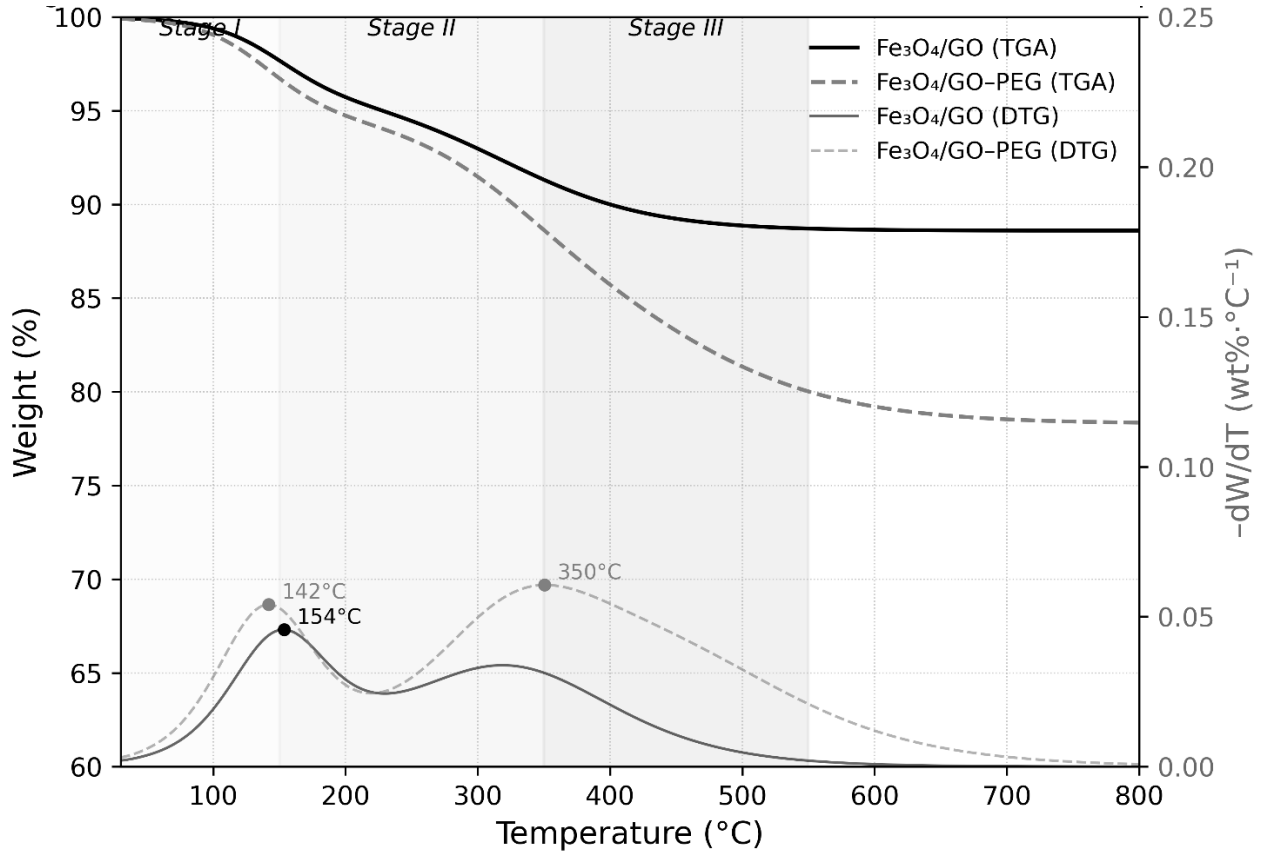

Figure 9 TGA–DTG curves of Fe_3O_4/GO and Fe_3O_4/GO–PEG nanocomposites.

The first weight-loss stage (30 - 150 °C) corresponds to the removal of physisorbed and interlayer water molecules. Both samples show a minor mass loss (< 6%), indicating low surface moisture. The second stage (150 - 350 °C) is attributed to the thermal decomposition of oxygen-containing functional groups (–OH, –COOH, and C=O) on the GO surface. This process involves the decarboxylation, dehydroxylation, and partial reduction of GO, resulting in the evolution of CO_2 and CO. In Fe_3O_4/GO–PEG, a distinct third stage (350 - 550 °C) appears, corresponding to the degradation of PEG chains through cleavage of C–O–C and C–H bonds in the polymer backbone. Beyond 600 °C, both samples exhibit negligible mass loss, confirming the formation of a thermally stable Fe_3O_4 spinel residue that remains intact up to 800 °C [55].

The DTG profiles exhibit characteristic peaks that identify maximum decomposition rates (T_{max}). Fe_3O_4/GO shows two DTG peaks at 125 °C (water desorption) and 325 °C (oxidation of GO). In contrast, Fe_3O_4/GO–PEG exhibits three distinct peaks at 120, 330 and 435 °C, corresponding to the sequential loss of water, decomposition of GO functional groups, and degradation of PEG chains, respectively. The emergence of the high-temperature DTG peak ($T_{max} \approx$ 435 °C) is a clear signature of PEG's thermal decomposition, confirming its covalent incorporation and stable interaction with the Fe_3O_4/GO matrix [56].

The slightly higher decomposition onset temperature (~340 °C) and the presence of the high-T_{max} DTG peak (~435 °C) suggest that PEG chains are not merely physically adsorbed but chemically bonded via Fe–O–C coordination and amide linkages, as evidenced by FTIR analysis. Such strong interfacial bonding enhances the overall thermal stability and cohesion of the composite matrix [57].

At temperatures exceeding 600 °C, the retained mass (> 75%) corresponds to the Fe_3O_4 crystalline residue, indicating the excellent thermal endurance of the magnetic core, even after repeated ultrasonic and enzymatic processing cycles. These findings are consistent with BET results (slightly reduced surface area due to partial pore filling by PEG) and ICP–OES data (reduced Fe leaching), collectively confirming that PEG acts as an interfacial stabilizer — improving both the chemical robustness and hydrophilic dispersion of the Fe_3O_4/GO–PEG nanocomposite.

Fe leaching resistance (ICP–OES)

The chemical stability and reusability of Fe_3O_4/GO and Fe_3O_4/GO–PEG nanocomposites under ultrasonic conditions were evaluated through iron leaching tests using inductively coupled plasma–optical emission spectroscopy (ICP–OES). The Fe concentration in the supernatant was quantified after sonication at 250 W for 30 min at 50 °C, and the results are summarized in **Figures 10(a) - 10(b)**.

As illustrated in **Figure 10(a)**, Fe_3O_4/GO exhibited a dissolved iron concentration of 6.0 ± 0.3 ppm, while Fe_3O_4/GO–PEG showed a significantly lower value of 2.8 ± 0.2 ppm—representing an approximate 53% reduction in Fe leaching after PEG modification. This improvement is attributed to the formation of a hydrated PEG barrier layer that envelops both Fe_3O_4 nanoparticles and GO sheets, minimizing solvent-induced oxidation and dissolution during ultrasonic exposure [58].

In the unmodified Fe_3O_4/GO composite, ultrasonic cavitation generates microjets and localized heating, promoting Fe^{2+}/Fe^{3+} oxidation–reduction cycles and partial detachment of nanoparticles from the GO matrix. The PEG coating mitigates these effects by stabilizing Fe–O–C interfacial linkages and reducing interfacial friction, thereby enhancing mechanical and chemical resistance under high-energy sonication [59].

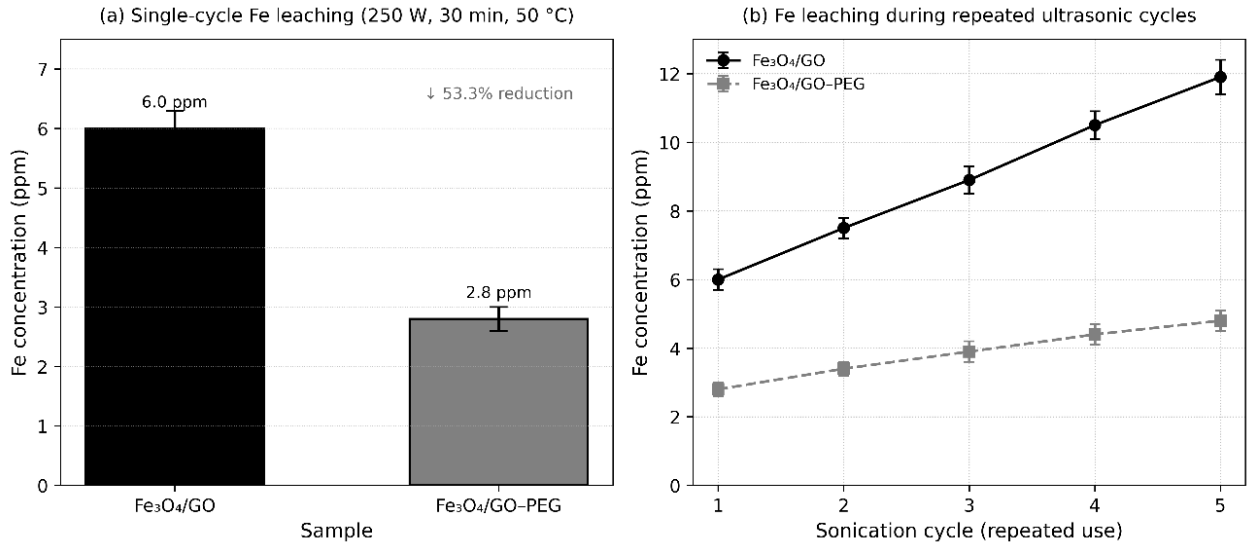

Figure 10 (a) Fe leaching resistance of Fe_3O_4/GO and (b) Fe_3O_4/GO–PEG nanocomposites measured by ICP–OES.

The reusability test over 5 consecutive sonication cycles (**Figure 10(b)**) further demonstrates the durability of the PEG-modified system. Fe_3O_4/GO exhibited a continuous increase in Fe concentration—from 6.0 ppm (cycle 1) to 11.9 ppm (cycle 5)—indicating progressive structural degradation and Fe dissolution due to cavitation fatigue [60]. In contrast, Fe_3O_4/GO–PEG maintained low Fe concentrations throughout the cycles, increasing only from 2.8 to 4.8

ppm, corresponding to roughly a 60% reduction in cumulative Fe release compared to Fe_3O_4/GO.

This sustained low Fe dissolution confirms that PEG functionalization significantly improves long-term chemical stability and reusability, effectively preventing nanoparticle agglomeration, shielding Fe active sites from oxidation, and preserving magnetic integrity under repeated ultrasonic conditions.

Schematic Illustration and mechanistic interpretation of Fe_3O_4/GO–PEG Stabilization

The stabilization of Fe_3O_4 nanoparticles within the GO–PEG matrix results from the synergistic action of Fe–O–C coordination, hydrogen bonding, and steric protection, which collectively maintain structural, magnetic, and colloidal integrity under ultrasonic conditions. The mechanism is conceptually illustrated in **Figure 11**.

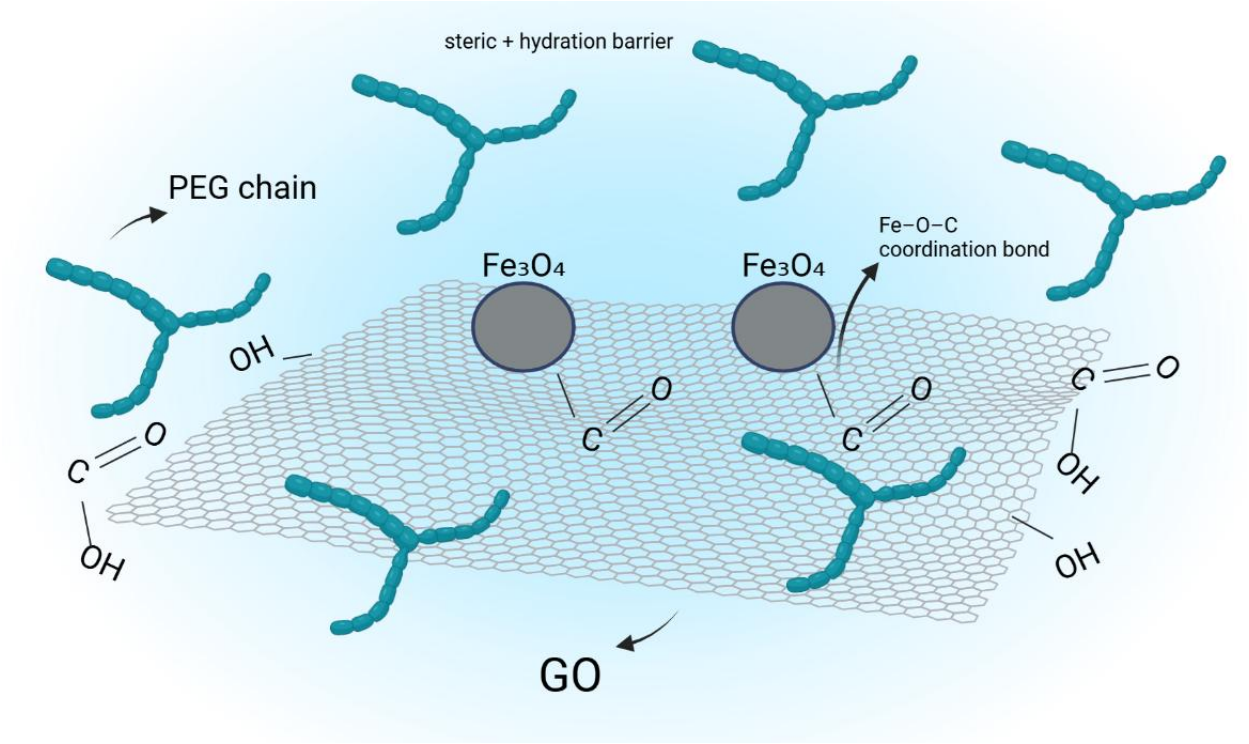

Figure 11 Schematic illustration of the stabilization mechanism in Fe_3O_4/GO–PEG nanocomposite.

During co-precipitation, oxygen-containing functional groups on graphene oxide (–COOH, –OH, and –C–O–C) coordinate with Fe^{2+}/Fe^{3+} ions, forming Fe–O–C linkages that firmly anchor Fe_3O_4 nanoparticles on the GO surface. The wrinkled morphology and high aspect ratio of GO introduce mechanical interlocking points, enhancing load distribution and preventing nanoparticle migration or aggregation [61].

Polyethylene glycol (PEG) chains subsequently adsorb onto Fe_3O_4 and GO through hydrogen bonding and weak coordination with surface oxygen atoms. These polymeric chains form a hydrated steric layer that minimizes magnetic dipole interactions and van der Waals attraction, thereby suppressing nanoparticle agglomeration. In addition, PEG's ether and hydroxyl groups facilitate water-mediated solvation, ensuring long-term dispersion stability [62].

The PEG layer also acts as a diffusion barrier against oxygen and hydroxyl radicals generated during ultrasonication, effectively reducing Fe^{2+}/Fe^{3+} oxidation and Fe-leaching reactions—consistent with ICP–OES data showing ~53% lower Fe release in Fe_3O_4/GO–PEG compared to unmodified Fe_3O_4/GO. Overall, these interactions establish a hierarchical stabilization network consisting of:

1) Fe–O–C coordination bonds ensure robust chemical anchoring,

2) hydrogen bonding links PEG chains with GO and Fe_3O_4 surfaces, and

3) steric repulsion from PEG provides physical separation and hydration.

This tri-level stabilization maintains the superparamagnetic behavior, thermal resistance, and aqueous dispersibility of the nanocomposite, as demonstrated by VSM, TGA, and DLS analyses. The schematic representation in **Figure 11** conceptually integrates these phenomena, linking structural chemistry to the experimentally observed physicochemical performance.

Comparative evaluation with reported Fe_3O_4-based nanocomposites

To validate the performance and structural advantages of the synthesized Fe_3O_4/GO–PEG nanocomposite, its key physicochemical and magnetic properties were compared with related Fe_3O_4-based systems, including Fe_3O_4/GO, Fe_3O_4@ZIF, and Fe_3O_4/GO–PVP composites. The comparison summarized in **Table 6** highlights the distinct balance between surface area, magnetic response and Fe-retention stability achieved by the Fe_3O_4/GO–PEG system under ultrasonic conditions.

Table 6 Comparative physicochemical and magnetic properties of Fe_3O_4-based nanocomposites from recent studies.

Material system	Surface area ($m^2\ g^{-1}$)	Particle Size (nm)	M_s (emu g^{-1})	Fe-Retention/ Stability	Notable features	Reference
Fe_3O_4/GO–PEG	112.4	7 - 15	55.8	High (≈ 53 % less Fe leaching under sonication)	High magnetic stability; PEG steric protection; strong Fe–O–C bonding	(This work)
Fe_3O_4/GO	135.0	10 - 20	63.2	Moderate; Fe leaching under aqueous sonication	Good dispersion but limited oxidation resistance	[63]
Fe_3O_4@ZIF	150.2	15 - 25	47.5	Moderate; ZIF shell partially decomposes under ultrasound	High surface area, lower magnetic response	[64]
Fe_3O_4/GO–PVP	102.3	12 - 18	52.0	High	PVP forms thin shell but less stable > 60 °C	[2]

As shown in **Table 6**, the Fe_3O_4/GO–PEG nanocomposite demonstrates a balanced physicochemical profile, combining moderate surface area (≈112 $m^2 \cdot g^{-1}$) with strong magnetic responsiveness (M_s = 55.8 emu·g^{-1}) and superior Fe-retention stability (~ 53% less Fe leaching than Fe_3O_4/GO). While Fe_3O_4@ZIF exhibits higher surface area due to its microporous framework, it suffers from lower magnetization and partial decomposition under ultrasonication. Conversely, PEG-functionalized composites—including this work—maintain magnetic integrity and resist oxidative degradation, underscoring the advantage of polymer-induced steric stabilization.

Collectively, these comparative findings confirm that PEG functionalization introduces a synergistic stabilization mechanism combining Fe–O–C coordination, hydrogen bonding, and hydrated steric shielding. This interaction network effectively prevents nanoparticle aggregation, enhances dispersion stability, and preserves magnetic recovery efficiency. Consequently, Fe_3O_4/GO–PEG represents a versatile, magnetically recoverable and aqueous-stable nanoplatform, exhibiting high structural integrity and reusability in both ultrasonic-assisted delignification and biocatalytic processes.

Conclusions

The Fe_3O_4/GO–PEG nanocomposite was successfully synthesized via a co-precipitation route followed by PEG-assisted surface functionalization, producing a magnetically recoverable, hydrophilic, and structurally stable hybrid nanomaterial. Comprehensive characterization confirmed the coexistence of crystalline Fe_3O_4 and GO phases, along with the effective chemical incorporation of PEG on the composite surface.

XRD analysis verified the retention of the inverse spinel structure of Fe_3O_4 with slight lattice contraction ($\Delta a \approx -0.24\%$), indicating interfacial strain and Fe–O–C coordination bonding with GO. TEM observations showed uniformly distributed Fe_3O_4 nanoparticles (7 - 15 nm) anchored on wrinkled GO sheets, while FTIR spectra evidenced Fe–O–C coordination, amide linkage formation, and hydrogen-bond interactions among Fe_3O_4, GO, and PEG. BET–BJH analyses revealed that PEG incorporation slightly decreased surface area and pore volume but preserved the mesoporous architecture, favorable for catalytic and enzyme immobilization functions.

Magnetic characterization (VSM) confirmed superparamagnetic behavior with a saturation magnetization of 55.8 $emu \cdot g^{-1}$, ensuring efficient magnetic separability. DLS and zeta potential measurements demonstrated that PEG functionalization imparted steric stabilization, enhancing colloidal stability ($\zeta = -8.3$ mV, stable > 7 days). Thermal and chemical stability were also markedly improved, evidenced by a higher decomposition onset temperature in TGA and approximately 53% reduction in Fe leaching (ICP–OES).

Overall, the Fe_3O_4/GO–PEG nanocomposite exhibits a synergistic combination of crystallinity, mesoporosity, magnetic responsiveness, and aqueous durability. These integrated properties position it as a promising candidate for recyclable catalytic systems in ultrasonic-assisted delignification and as a robust carrier for cellulase immobilization in SHF or SSF bioethanol production. The established structure–property correlation provides a fundamental basis for advancing the design of magnetically recoverable nanocomposites with optimized physicochemical and catalytic performance in future studies.

Acknowledgements

The authors would like to express their sincere gratitude to the Biomass Processing Technology Laboratory, Faculty of Engineering, Universitas Negeri Semarang, Indonesia for providing the research facilities and technical support necessary for conducting this study.

Declaration of Generative AI in Scientific Writing

The authors recognize that generative AI tools (such as QuillBot and OpenAI's ChatGPT) were utilized during the preparation of this manuscript, solely to assist with language refinement and gramma editing. No sections of the content were generated, nor was any data interpreted, by AI. The authors assume complete responsibility for the work's content and the conclusions drawn

CRediT Author Statement

Hanif Ardhiansyah: Conceptualization, Data curation, Formal analysis, Investigation, Methodology, Writing –original draft, writing – review & editing. **Tutuk Djoko Kusworo:** Supervise methodology, conceptualization, data curation, formal analysis, and writing – review & editing. **Andri Cahyo Kumoro:** Supervise, methodology, conceptualization, data curation, formal analysis, writing – review & editing.

References

[1] M Moghaddam-Manesh, R Darvishi, A Barati, A Moshkriz and M Seyedsharifi. Synthesis of novel Fe3O4@gly@Indole@CuNO3 magnetic nanoparticle as high-performance antibiotic absorbent, antimicrobial agent, and reusable magnetic Nano catalyst. *Journal of Environmental Chemical Engineering* 2025; **13(1)**, 114970.

[2] SIA Shah, W Ahmad, M Anwar, R Shah, JA Khan, NS Shah, A Al-Anazi and C Han. Synthesis, properties, and applications of Fe3O4 and Fe3O4-based nanocomposites: A review. *Applied Catalysis O: Open* 2025; **203**, 207049.

[3] RF Abbas, MJM Hassan and AM Rheima. Adsorption of fast green dye onto Fe3O4 MNPs and GO/Fe3O4 MNPs synthesized by photo-irradiation method: Isotherms, thermodynamics, kinetics, and reuse studies. *Sustainable Chemistry for the Environment* 2024; **6**, 100104.

[4] AN Ghulam, OAL Santos, L Hazeem, BP Backx, M Bououdina and S Bellucci. Graphene oxide (GO) materials—applications and toxicity on living organisms and environment. *Journal of Functional Biomaterials* 2022; **13(2)**, 77.

[5] TD Kusworo, M Yulfarida, AC Kumoro and DP Utomo. Purification of bioethanol fermentation broth using hydrophilic PVA crosslinked PVDF-

GO/TiO2 membrane. *Chinese Journal of Chemical Engineering* 2023; **55**, 123-136.

[6] C Donga, SB Mishra, LN Ndlovu, AS Abd-El-Aziz, AT Kuvarega and AK Mishra. Magnetic magnetite-graphene oxide (Fe3O4-GO) nanocomposites for removal of dyes from aqueous solution. *Journal of Inorganic and Organometallic Polymers and Materials* 2024; **34**, 4192-4202.

[7] M Popova, N Koseva, I Trendafilova, H Lazarova, V Mitova, J Mihály, D Momekova, S Konstantinov, IZ Koleva, PS Petkov, GN Vayssilov, HA Aleksandrov and Á Szegedi. Design of PEG-modified magnetic nanoporous silica based miltefosine delivery system: Experimental and theoretical approaches. *Microporous and Mesoporous Materials* 2021; **310**, 110664.

[8] RA Abdul-Nabi and E Al-Bermany. Fabrication of antibiofilm-based-polymer nanocomposite for biophysical applications. *Trends in Sciences* 2025; **22(6)**, 9762.

[9] G Antarnusa and E Suharyadi. A synthesis of polyethylene glycol (PEG)-coated magnetite Fe3O4 nanoparticles and their characteristics for enhancement of biosensor. *Materials Research Express* 2020; **7(5)**, 56103.

[10] SI Bernad, A Bunge, MC Ioncica, R Turcu, M Dan, V Socoliuc, D Susan-Resiga and ES Bernad. Impact of the different molecular weights of polyethylene glycol (PEG) coating agents on the magnetic targeting characteristics of functionalized magnetoresponsive nanoclusters. *Magnetochemistry* 2024; **10(7)**, 51.

[11] A Cahyo Kumoro and MTMN Saeed. Ultrasound-assisted transesterification of tropical goat fat – Palm oil blend for biodiesel synthesis. *Energy Conversion and Management: X* 2022; **14**, 100213.

[12] Y Bao, H Li, J He, K Song, H Yu, C Tian, J Guo, X Zhou and S Liu. Polyethylene glycol modified graphene oxide-silver nanoparticles nanocomposite as a novel antibacterial material with high stability and activity. *Colloids and Surfaces B: Biointerfaces* 2023; **229**, 113435.

[13] RS Shinde, VA Adole, SD Khairnar, PB Koli and TB Pawar. Study of Fe3O4 and Cu2+ doped modified Fe3O4 nano catalyst for photocatalytic degradation of methylene blue and eriochrome black-T dyes: Synthesis, characterization, and antimicrobial assessment. *Inorganic Chemistry Communications* 2024; **170**, 113206.

[14] PK Jha, C Chawengkijwanich, K Techato, W Limbut and M Luengchavanon. Callistemon viminalis Leaf Extract Mediated Biosynthesis of Ag, rGO-Ag-ZnO Nanomaterials for Catalytic PEM Fuel Cell Application. *Trends in Sciences* 2022; **19(11)**, 493.

[15] MS Jamal, MS Chowdhury, S Bajgai, M Hossain, A Laref, PK Jha and K Techato. Comparative studies on the morphological, structural and optical properties of NiO thin films grown by vacuum and non-vacuum deposition techniques. *Materials Research Express* 2021; **8(12)**, 12604.

[16] TD Kusworo, F Dalanta, DA Azizah, AN Putra, TP Hendratmo, MI Hanif, I Alkian and TA Kurniawan. Integrated ultrafiltration and pervaporation process using PDMS/ZnO-modified PSf nanohybrid membranes for enhanced bioethanol purification from fermentation broth. *Case Studies in Chemical and Environmental Engineering* 2025; **12**, 101278.

[17] D Nematov. Titanium dioxide and photocatalysis: A detailed overview of the synthesis, applications, challenges, advances and prospects for sustainable development. *Journal of Modern Green Energy* 2024; **3**, 6.

[18] DD Nematov, AS Burkhonzoda, KT Kholmurodov, AI Lyubchyk and S Lyubchyk. Study on structural stability of ZrO2 and YSZ: Doping-induced phase transitions and fermi level shift. *Advanced Energy Conversion Materials* 2023. https://www.preprints.org/manuscript/202308.0586/v2

[19] C Reuter and S Strehle. Sub-10 nm oxidation and etching of graphite using field emission scanning Probe lithography. *Carbon* 2025; **245**, 120779.

[20] C Cai, N Sang, Z Shen and X Zhao. Facile and size-controllable preparation of graphene oxide nanosheets using high shear method and ultrasonic method. *Journal of Experimental Nanoscience* 2017; **12(1)**, 247-262.

[21] J Park, W Lee, J Nam, JT Han, CJ Choi and J Hwang. A study of the correlation between the oxidation degree and thickness of graphene oxides. *Carbon* 2022; **189(9)**, 579-585.

[22] P Soltanpour, R Naderali and K Mabhouti. Comparative study on structural, morphological, and optical properties of MS/Fe3O4 nanocomposites and M-doped Fe3O4 nanopowders (M = Mn, Zn). *Scientific Reports* 2024; **14(1)**, 21287.

[23] VV Balashev, KS Ermakov, AY Samardak, AV Ognev, AS Samardak, SV Komogortsev, MN Volochaev, AS Tarasov and VV Korobtsov. Crystal texture-dependent magnetic and magnetotransport properties of half-metallic Fe3O4 films grown on oxidized Si substrates by reactive deposition. *Journal of Alloys and Compounds* 2020; **815**, 152398.

[24] SJ Ahmed and E Al-Bermany. Multiscale characterization and optical and radiation absorption behavior of hybrid nanocomposites for advanced applications. *Trends in Sciences* 2025; **22(10)**, 10659.

[25] MK Shahid and Y Choi. Characterization and application of magnetite Particles, synthesized by reverse coprecipitation method in open air from mill scale. *Journal of Magnetism and Magnetic Materials* 2020; **495**, 165823.

[26] S Devesa, AP Rooney, MP Graça, D Cooper and LC Costa. Williamson-hall analysis in estimation of crystallite size and lattice strain in Bi1.34Fe0.66Nb1.34O6.35 prepared by the sol-gel method. *Materials Science and Engineering: B* 2021; **263**, 114830.

[27] WM Ng and JK Lim. Complex interplay between colloidal stability, transport, chemical reactivity and magnetic separability of polyelectrolyte-functionalized nanoscale zero-valent iron particles (nZVI) toward their environmental engineering application. *Colloid and Interface Science Communications* 2022; **46**, 100582.

[28] MA Rahaman, MT Islam, S Aman, MM Rahman, A Ahmad, RT Tama, U Podder, M Al-Amin and MA Alam. Crystallographic phase bibliography and quantitative phase analysis of TiO2 nanocrystals: A rietveld refinement insight. *Next Research* 2025; **2(3)**, 100469.

[29] H Qiao, G Sudre, A Maazouz and K Lamnawar. Industrial crops & products dual enhancement of dispersion of cellulose nanocrystals, crystallization performance, flexibility and barrier properties through polyethylene glycol coating in melt-processed poly (L-lactide) -based nanocomposites. *Industrial Crops and Products* 2025; **224**, 120337.

[30] W Li, Y Zhao, Y Liu, W Yan, Z Chen and W Yang. Preparation and catalytic performance of porous magnetically recyclable Fe3O4@ZIF-8@Cux/Pdy catalyst. *Journal of Physics and Chemistry of Solids* 2025; **205**, 112807.

[31] S Hegazy, NA Abdelwahab, AM Ramadan and SK Mohamed. Magnetic Fe3O4-grafted cellulose/graphene oxide nanocomposite for methylene blue removal from aqueous solutions: Synthesis and characterization. *Next Materials* 2024; **3**, 100064.

[32] L Chen, C Zhu, Y Si, Q Yang, X Chen and C Zhou. Enhanced electromagnetic wave absorption performance of multi-layer Fe3O4@rGO composite absorber. *Applied Surface Science* 2025; **688**, 162434.

[33] S Wang, Y Feng, M Hu and H Sun. In-situ electrocatalytic degradation of PEG-6000 via 3D system with waste-activated carbon Ni-Mn BPEs: Mechanism, factors, and regeneration. *Journal of Environmental Chemical Engineering* 2025; **13(2)**, 115529.

[34] M Brogly, S Bistac and D Bindel. Adsorption and Structuration of PEG Thin Films: Influence of the Substrate Chemistry. *Polymers* 2024; **16(9)**, 1244.

[35] P Basnet, PK Jha, A Gupta and S Chatterjee. Synergistic effect of tea-phytochemicals, noble metals and Zno Nano-Photo-Composites for combating resistance of bacterial growth. *Journal of Nano Research* 2021; **70**, 53-66.

[36] PK Jha, W Khongnakorn, C Chawenjkigwanich, MS Chowdhury and K Techato. Eco-friendly reduced graphene oxide nanofilter preparation and application for iron removal. *Separations* 2021; **8(5)**. 68.

[37] MD Nguyen, HV Tran, S Xu and TR Lee. Fe3O4 Nanoparticles: Structures, synthesis, magnetic properties, surface functionalization, and

emerging applications. *Applied Sciences* 2021; **11(23)**, 11301.

[38] N Abbasi, SA Khan, Z Liu and TA Khan. Natural deep eutectic solvent (fructose-glycine) functionalized-celite/ polyethylene glycol hydrogel nanocomposite for phosphate adsorption: Statistical analysis. *Journal of Environmental Management* 2023; **330**, 117206.

[39] L He, J Zhou, D Liu, Y Wen and Y Gan. Preparation of Fe3O4@GO@MIL-101 nanocomposites and efficient degradation of oxytetracycline hydrochloride by promoting charge separation during the photo-Fenton process. *Materials Science in Semiconductor Processing* 2024; **172**, 108050.

[40] N Fattahi, J Reed, E Heronemus, P Fernando, R Hansen and P Parameswaran. Polyethylene glycol hydrogel coatings for protection of electroactive bacteria against chemical shocks. *Bioelectrochemistry* 2024; **156**, 108595.

[41] SG Hong, E Im, DI Kim, EJ Jeong, J Kim, GD Moon and DC Hyun. Magnetic polymer bowl for enhanced catalytic activity and recyclability. *RSC Advances* 2021; **11(22)**, 13545-13555.

[42] X Hu, Z Qiu, M Huang, J Jiang, J Wei, X Mou, Y Xie, J Qi and C Zou. Fe3O4@APTES@CB[7] supramolecular cascade catalyst with tunable morphology for aniline removal in wastewater. *Journal of Environmental Chemical Engineering* 2025; **13(1)**, 115026.

[43] CM Zhang, YZ Qiu, H Wu, J Guan, SG Wang and XF Sun. Polyethylene glycol-polyvinylidene fluoride/TiO2 nanocomposite polymer coatings with efficient antifouling strategies: Hydrophilized defensive surface and stable capacitive deionization. *Journal of Colloid and Interface Science* 2024; **666**, 585-593.

[44] J Waluyo, FC Abimanyu, FY Widharmo, SH Pranolo, M Kaavessina, I Kurnia and IT Purba. Co-precipitated magnetic graphene oxide nanocomposites for methyl orange uptake: Isotherm, kinetic, and regeneration. *Results in Chemistry* 2025; **18**, 102790.

[45] Z Sun, W Zhao, J Wu, K Shi, L Zhang and W Kou. One-step hydrothermal synthesis of Fe3O4/GO composites combined with persulfate for the removal of reactive black in aqueous solution. *Bulletin of Chemical Reaction Engineering and Catalysis* 2025; **20(3)**, 392-402.

[46] H Baniasadi, Z Fathi, R Abidnejad, PES Silva, S Bordoloi, J Vapaavuori, J Niskanen, E Lizundia, E Kontturi and J Lipponen. Biochar-infused cellulose foams with PEG-based phase change materials for enhanced thermal energy storage and photothermal performance. *Carbohydrate Polymers* 2025; **367**, 123999.

[47] MS Raghu, K Yogesh Kumar, MK Prashanth, BP Prasanna, R Vinuth and CBP Kumar. Adsorption and antimicrobial studies of chemically bonded magnetic graphene oxide-Fe3O4 nanocomposite for water purification. *Journal of Water Process Engineering* 2017; **17**, 22-31.

[48] Y Cheng, S Yang and E Tao. Magnetic graphene oxide prepared via ammonia coprecipitation method: The effects of preserved functional groups on adsorption property. *Inorganic Chemistry Communications* 2021; **128**, 108603.

[49] A Bertran, S Sandoval, J Oró-Solé, À Sánchez and G Tobias. Particle size determination from magnetization curves in reduced graphene oxide decorated with monodispersed superparamagnetic iron oxide nanoparticles. *Journal of Colloid and Interface Science* 2020; **566**, 107-119.

[50] M Hartyányi, R Nagy, R Bejczi, L Bartha and S Puskás. Estimation of the hydrodynamic diameter of mobility-controlling polymers for chemical enhanced oil recovery based on dynamic viscosity. *Heliyon* 2025; **11(13)**, e43709.

[51] F Matter, AL Luna and M Niederberger. From colloidal dispersions to aerogels: How to master nanoparticle gelation. *Nano Today* 2020; **30**, 100827.

[52] Y Ma, M Zohaib Aslam, M Wu, N Nitin and G Sun. Strategies and perspectives of developing anti-biofilm materials for improved food safety. *Food Research International* 2022; **159**, 111543.

[53] LM Ande and MS Reddy. PEG-functionalized ZnO nanoparticles synthesized by Co-precipitation for improved antibacterial performance. *Journal of the Indian Chemical Society* 2025; **102(11)**, 102107.

[54] O Bongomin, C Nzila, JI Mwasiagi and O Maube. Comprehensive thermal properties, kinetic, and thermodynamic analyses of biomass wastes

pyrolysis via TGA and Coats-Redfern methodologies. *Energy Conversion and Management: X* 2024; **24**, 100723.

[55] Q Xie, F Liu, Y Zhong, C Li and Y Ding. Thermal degradation of peeled cotton stalk with thermogravimetry/fourier transform infrared analysis and shuffled complex evolution algorithm. *Biomass Bioenergy* 2025; **198**, 107853.

[56] J Li, H Wang, G Liu, T He, Z Wang, J Wuabc and J Wu. Facile synthesis of hierarchical nanocrystalline H[Fe,Al]ZSM-5 with boosted lifetime for DTG reactions. *Catalysis Science & Technology* 2024; **14(19)**, 5588-5598.

[57] M Chen, H Yu, K Wang, Binbin Yao, D Zhang, T Cui, Y Yue, W Huo, H Ma, S Song and S Zhang. Study on the thermal decomposition characteristics of different carbohydrates by TG-FTIR-GC/MS. *Carbohydrate Research* 2025; **558**, 109680.

[58] Erdiwansyah, A Gani, H Desvita, Mahidin, Bahagia, R Mamat and SM Rosdi. Investigation of heavy metal concentrations for biocoke by using ICP-OES. *Results in Engineering* 2025; **25**, 103717.

[59] V Nishad, S Kumar and SVAR Sastry. A review on heavy metals removal using zerovalent iron nanoparticles: Synthesis, mechanism, applications, and challenges. *Trends in Sciences* 2025; **22(5)**, 9702.

[60] EA Mends, SE Arthur, S Hussaini, JS Thella and P Chu. Investigating the selective extraction of metals from nickel sulfide tailings using salt roasting and acid leaching. *Minerals Engineering* 2025; **231**, 109433.

[61] AI Mugisha, C Fauteux-Lefebvre, P Thangarasu and CA Huerta-Aguilar. Two-dimensional graphene oxide-iron oxide catalysts for oxidation of sulfides: Synthesis, product analysis, and environmental impact. *Journal of Molecular Structure* 2025; **1339**, 142382.

[62] R Eshraghi, M Fasihi and A Ghaemi. Optimization of PEG-modified phenolic foam for enhanced CO2 adsorption: A micro-meso structural approach. *Results in Engineering* 2025; **26**, 104864.

[63] HL Zhang and S Chao. Fe_3O_4/GO-Zn Magnetic nanocatalyst: A recyclable and efficient catalyst for the green synthesis of 2,4,6-Triarylpyridines via multicomponent reactions. *Journal of Synthetic Chemistry* 2025; **4(3)**, 222-238.

[64] X Wei, Y Ye, W Cai and Z Chen. Innovative pH-responsive C-Fe_3O_4@ZIF-8 composites: A dual-advantage approach for enhanced drug delivery and environmental sustainability. *Inorganic Chemistry Communications* 2026; **183**, 115737.